https://doi.org/10.5194/egusphere-2023-657
Preprint. Discussion started: 12 April 2023

Array processing in cryoseismology

Thomas S. Hudson[1], Alex M. Brisbourne[2], Sofia-Katerina Kufner[3], J-Michael Kendall[1], and Andy M. Smith[2]

[1]Department of Earth Sciences, University of Oxford, 3 South Parks Rd, Oxford, OX1 3AN, UK
[2]UKRI NERC British Antarctic Survey, High Cross, Madingley Rd, Cambridge CB3 0ET, UK
[3]Geophysical Institute, Karlsruhe Institute of Technology, 76131 Karlsruhe, Germany

Correspondence: Thomas S. Hudson (thomas.hudson@earth.ox.ac.uk)

Abstract.

Seismicity at glaciers, ice sheets and ice shelves provides observational constraint of a number of glaciological processes. Detecting and locating this seismicity, specifically icequakes, is a necessary first step in studying processes such as basal slip, crevassing, and imaging ice fabric, for example. Most glacier deployments to date use conventional seismic networks, comprised of seismometers distributed over the entire area of interest. However, smaller aperture seismic arrays can also be used, which are typically sensitive to seismicity distal from the array footprint and require a smaller number of instruments. Here, we investigate the potential of arrays and array-processing methods to detect and locate seismicity in the cryosphere, benchmarking performance against conventional seismic network-based methods. We also provide an array-processing recipe for cryosphere applications. Results from an array and network deployed at Rutford Ice Stream, Antarctica, show that arrays and networks both have strengths and weaknesses. Arrays can detect icequakes from further distances whereas networks outperform arrays for more comprehensive studies of a process within the network extent, due to greater hypocentral constraint and a smaller magnitude of completeness. We also gain new insights into seismic behaviour at Rutford Ice Stream. The array detects basal icequakes in what was previously interpreted to be an aseismic region of the bed, as well as new icequake observations at the ice stream shear-margins, where it would be challenging to deploy instruments. Finally, we make some practical recommendations for future array deployments at glaciers.

1 Introduction

Cryoseismology is a rapidly emerging field that shows promise for studying glaciological processes (Podolskiy and Walter, 2016; Aster and Winberry, 2017). For example, icequakes associated with basal slip (Smith et al., 2015; Roeoesli et al., 2016; Kufner et al., 2021) can provide observational constraint of frictional processes in ice dynamics models (Gräff and Walter, 2021; Hudson et al., 2023, 2020; Köpfli et al., 2022; Lipovsky et al., 2019; Zoet et al., 2013). However, glaciers are often challenging to access, logistically expensive to operate within and potential seismically active areas are typically highly variable temporally and spatially. To date, detecting such icequakes has generally been performed using conventional, network-based detection and location methods. Conventional seismic networks typically require receiver spacings similar to the distance of the events from the receiver and are primarily only sensitive to icequakes within the spatial extent of the

https://doi.org/10.5194/egusphere-2023-657
Preprint. Discussion started: 12 April 2023

network. Therefore, adequately sampling a specific region may require tens to hundreds of receivers. Conversely, seismic arrays are sensitive to icequakes outside the array aperture, with individual arrays requiring significantly fewer instruments than a conventional network. Seismic arrays could therefore facilitate smaller seismic deployments than conventional networks, while enabling event detection at greater distances. Here, we address the question: to what extent are array deployments useful for icequake studies. Specifically, we assess the sensitivity of arrays compared to networks for: icequake detection; icequake location; whether arrays can detect event types typically missed by standard network-based detection algorithms; and discuss the limitations of arrays compared to networks.

Array processing has existed as a method for decades. The core component of array processing, beamforming, involves combining plane-wave arrivals from all receivers in an array to find the direction of the origin of the wave from the array (Rost and Thomas, 2002). It was originally developed for nuclear test ban monitoring (Bowers and Selby, 2009), but has since been applied to other topics, including: studying the structure of the earth (Wolf et al., 2023; Wang and Vidale, 2022; **?**); monitoring offshore seismicity (Jerkins et al., 2023); ambient seismic noise source analysis (Bowden et al., 2021; Löer et al., 2018); and icequake detection using Distributed Acoustic Sensing instrumentation (Van Den Ende and Ampuero, 2021; Näsholm et al., 2022; Klaasen et al., 2021). However, the use of array processing within cryoseismology is limited. Beamforming has been used to locate large slip events at Whillans Ice Stream, Antarctica (Pratt et al., 2014). Multiple regional arrays have been used to locate glacier icequakes, likely caused by significant calving events (Ekström et al., 2003; Ekström, 2006; Tsai and Ekström, 2007). Array processing has also proven useful for locating glacier tremor (Lindner et al., 2020; Umlauft et al., 2021; McBrearty et al., 2020). The closest application to that investigated in this study is the work of Cooley et al. (2019), where beamforming is not used for icequake detection but is used for subsequent event location. Here, we present results of icequake detection and location solely using array processing and compare it to a conventional network-based approach, using a dataset from Rutford Ice Stream (RIS), Antarctica (see Figure 1).

2 Data

The dataset used in this study is from receivers deployed on the surface of RIS, Antarctica. The instruments deployed consist of sixteen 4.5 Hz geophones connected to Reftek RT130 dataloggers sampling at 1000 Hz, in the geometry shown in Figure 1. Ten of these instruments were deployed in a 90 m apperture array. They were deployed in the austral summer of 2019 to 2020. RIS flows at $\sim 400\ m\ yr^{-1}$, with the bed known to be seismically active from previous studies (Kufner et al., 2021; Smith et al., 2015; Smith, 2006; Hudson et al., 2021). RIS is therefore an ideal site with which to test array-based methods at glaciers.

3 Methods

3.1 Array processing

For the purposes of this study, we define a seismic array as a collection of seismic receivers configured in a geometry that allows for the data to be jointly processed using beamforming methods. In comparison, we define a network as a collection

https://doi.org/10.5194/egusphere-2023-657
Preprint. Discussion started: 12 April 2023

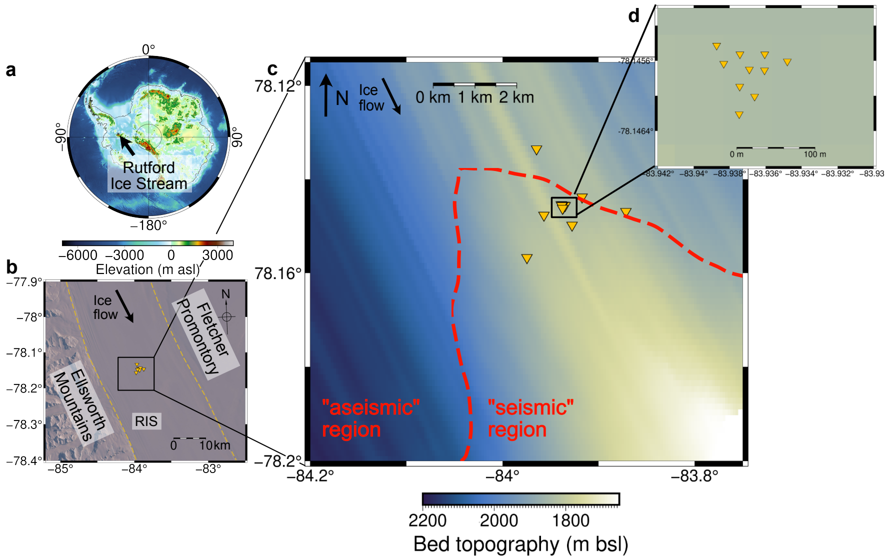

Figure 1. The seismic array deployment. a) Location of Rutford Ice Stream (RIS) with respect to Antarctica (basal topography is from Fretwell et al. (2013)). b) Overview of the deployment within RIS. c) Plot of the seismic network and array, as well as the previously assumed seismic and aseismic regions of the bed (Smith et al., 2015). d) Plot of array in detail.

of seismic receivers that are used to perform conventional seismic detection and location, spaced so as to be most sensitive to events inside the network.

3.1.1 Detection and location

There are several different methods for detecting and locating icequakes using arrays. Here, we describe the specific method chosen for this study, a frequency-domain, frequency-wavenumber (fk) beamforming method, chosen because it is more computationally efficient than time-domain methods (Rost and Thomas, 2002).

The method comprises of three overall steps (see Figure 2):

1. Compute the beam power, slowness and back-azimuth time-series ($P(t)$, $S(t)$, $\Theta(t)$).

2. Detect and associate icequake phase arrivals.

3. Locate each icequake (via either full-3D or fixed-depth methods).

$P(t)$, $S(t)$ and $\Theta(t)$ are calculated using the frequency-wavenumber method as follows. First, the discrete frequencies to perform beamforming on are specified. Here, we use 20 values between *10 Hz* and *150 Hz*, the bandwidth within which icequakes have previously been observed at RIS (Smith et al., 2015; Kufner et al., 2021). The slowness limits for the beamforming calculation are then defined. The maximum slowness for this study is defined as $1\ s\ km^{-1}$, which is chosen based on an extreme estimate of the minimum apparent velocity ($1\ km\ s^{-1}$) that one might expect to detect for an icequake at RIS. We also make

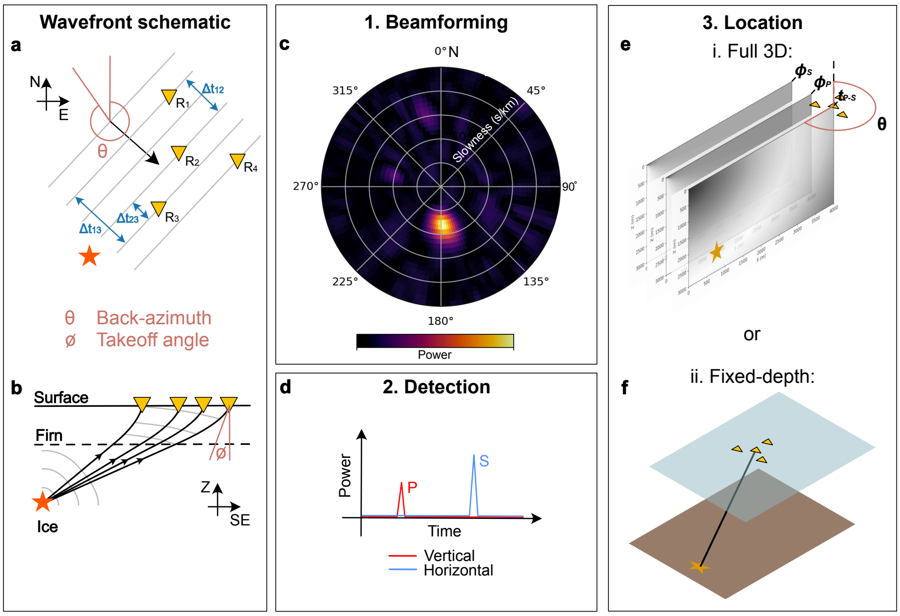

Figure 2. a,b. Plane wave arriving at array in the horizontal and vertical planes, respectively. All arrivals are time-shifted to align arrivals. (diagram inspired by Bowden et al. (2021)) c. Heatmap of beam power in slowness-back-azimuth space for one time window. An event is shown by the peak in power. d. Schematic example of power time-series, with vertical peaks associated with P arrivals and horizontal peaks with S arrivals. e. Array-based 3D location algorithm, involving stacking PDFs of P-S travel-time, P-wave takeoff angle and S-wave takeoff angle. f. Fixed depth array-based location using back-azimuth and P-S travel-time only.

the assumption of a plane wave incident at the array. This is approximately valid for a *90 m* aperture array with a minimum hypocentral distance of *2.2 km* (ice thicknes). The velocity time-series data at each receiver are then windowed in time, in order to calculate beam power, slowness and back-azimuth for each time window. The time window used here is *0.025 s*, the slowest time it would take for a seismic wave to travel across the array. The following steps are performed for each time window:

1. Calculate the power spectra for each receiver, for all three orthogonal components (Z, N, E).
2. Calculate the cross-correlation for phase shifts corresponding to each point in the 2D slowness domain (see Figure 2c).
3. The slowness data are then stacked over all discrete frequencies. Here we linearly stack the data (see Section 3.1.4 for more details).

One now has the power for all points in the 2D slowness space, for each time window (see Figure 2c). From this 2D slowness space, the peak power *P(t)* and its associated slowness *S(t)* and back-azimuth $\Theta(t)$ can be calculated for each window. This process is performed for the vertical and both horizontal components of the seismic data separately.

P(t), S(t) and Θ*(t)* can then be used to detect icequakes. For this study, the vertical component power time-series, $P_V(t)$, is used to detect potential P-wave arrivals and the two horizontal power time-series are summed to give $P_H(t)$, used to detect po-

https://doi.org/10.5194/egusphere-2023-657
Preprint. Discussion started: 12 April 2023

tential S-wave arrivals. Potential P- and S- wave arrivals are detected by searching for peaks in $P_V(t)$ and $P_H(t)$, respectively (see Figure 2d). This is performed using an median absolute deviation (MAD) threshold, with any peak in $P(t)$ with a MAD multiplier value > 15 (optimised for this dataset) and a time separation $> 0.25\ s$ defined as a potential phase arrival (based on the minimum P-S separation time for a basal icequake). Potential P- and S- phases then need to be associated. We only trigger an icequake detection if we can associate both P-wave and S-wave arrivals for an event. The phase association algorithm is as follows, with an example of the result shown in Figure 3a. First, only potential P and S arrivals with a maximum separation of $\Delta t_{P-S,max} = 2.5s$ are considered, to minimise mis-associating incorrect arrivals, although we increase this value to $\Delta t_{P-S,max} = 10s$ in an attempt to search for more distal icequakes in Section 4.3. The value of Δt_{P-S} used limits the hypocentral distance to which we can detect earthquakes (see Equation 1). In order to account for possible overlapping event arrivals, only P and S arrivals with back-azimuths in agreement within 10^o are paired. The third criteria is that the highest power P arrival is associated with the highest power S arrival that has a back-azimuth difference $< 10^o$ and a time difference $< \Delta t_{P-S}$, and so on for lower and lower power arrivals. In practice, the maximum-power criterion is rarely required, as two events are normally distinguishable within the $\Delta t_{P-S} = 2.5\ s$ window by back-azimuth alone.

The phase-associated icequake arrivals can then be used to locate events. Array-based icequake location differs from network-based methods in that instead of many P- and S- phase arrivals used to locate an event, one instead has single P and S arrival observations, but with the additional information of slowness and back-azimuth associated with these two phase arrivals. To use an array to locate an icequake in 3D, one has to calculate a takeoff angle and a radial distance, d_{EQ}, from the event to the receiver, in addition to using the back-azimuth. In this study, we compare two methods of finding icequake hypocentres: a 3D location method and a fixed-depth method (see Figure 2e,f). The motivations for applying these two methods are discussed in Section 4.2. In both cases, d_{EQ} is calculated using the P-S travel-time delay, Δt_{P-S}, using the equation,

$$d_{EQ} = \frac{v_P v_S}{v_P - v_S} \Delta t_{P-S}, \tag{1}$$

where v_P and v_S are the path-average P- and S-wave velocities, respectively. In the fixed depth method, the icequake location is calculated by projecting the distance d_{EQ} onto a fixed-depth horizontal plane at the measured back-azimuth (see Figure 2f). However, in the 3D location method the takeoff angle, as well as d_{EQ}, is required to derive the icequake depth (see Figure 2e). For a vertically homogeneous ice structure, the raypath from icequake source to receiver is linear, so the takeoff angle can be used to directly locate the event. However, at RIS there is a $\sim 100\ m$ thick firn layer directly below the surface, which has increasingly slow seismic velocities towards the surface (Smith et al., 2020; Zhou et al., 2022). This causes the rays to dip steeply vertical as they near the surface that has to be accounted for when locating icequakes. We therefore specify a vertically varying but laterally homogeneous velocity model and perform ray-tracing at *10 m* grid resolution to create a 2D spatial takeoff angle Probability Density Function (PDF) in depth and horizontal distance from the array. We then calculate d_{EQ} for a given icequake and assume a given uncertainty, δd_{EQ}, and create a 2D spatial PDF from d_{EQ}, again in depth and horizontal distance from the array, for d_{EQ}. The takeoff angle and d_{EQ} PDFs are then stacked and normalised (see Figure 2e), in order to find the most likely icequake location, defined as the peak in the combined PDF (see Figure 2e).

https://doi.org/10.5194/egusphere-2023-657
Preprint. Discussion started: 12 April 2023

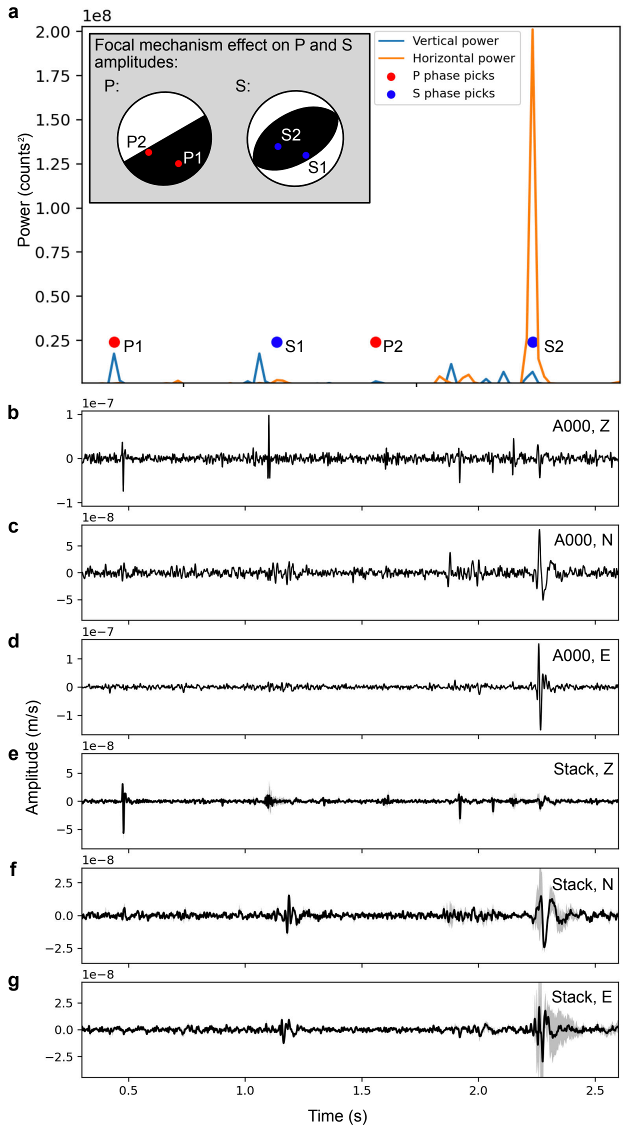

Figure 3. Example of array phase detection and association performance. a. Plot of power and peaks associated with phase arrivals for two events.n of an event alysis (FTAN) Inset diagram shows focal mechanism effects. b-d. Waveforms arriving at centre array station. e-g. Mean of stacked and time-shifted waveforms for the entire array, using the slowness and back-azimuth of event 2 in (a).

3.1.2 Uncertainty estimation

There are various sources of uncertainty in icequake phase arrival times and hypocentres. Sources include uncertainty in the velocity model, the GPS-derived receiver locations and potentially anisotropic effects. Here, we estimate the overall uncertainty
120 in event phase arrival times and location as follows. Phase arrival time uncertainties are defined as the full-width half maximum

https://doi.org/10.5194/egusphere-2023-657
Preprint. Discussion started: 12 April 2023

of the peak in the power time-series associated with the particular phase arrival. Spatial uncertainties are defined by uncertainty in slowness and back-azimuth. The uncertainty in slowness is defined as the full-width half maximum of the peak in power in the radial direction of the 2D slowness space (Figure 2c). Similarly, the uncertainty in back-azimuth is the full-width half maximum of the peak in power azimuthally in the 2D slowness space of Figure 2c. In each case, the full-width half maximum is used rather than the standard deviation of a Gaussian fit to improve computational efficiency. We assume that there is negligible uncertainty in the velocity model. However, in reality uncertainty in the velocity model will likely contribute to uncertainty in event locations that we have not accounted for in the array-processing derived icequake locations.

3.1.3 Array sensitivity

Seismic arrays are sensitive to icequakes with a particular bandwidth, which is governed by the minimum and maximum spacing between individual receivers. The minimum optimal frequency that an array is sensitive to is proportional to the maximum receiver spacing and vice versa for the maximum optimal frequency. The equation that describes this is given by (Bowden et al., 2021),

$$f = \frac{v}{x_{rec}}, \tag{2}$$

where f is frequency, v is the approximate seismic velocity and x_{rec} is the receiver spacing. For the array in this study, the minimum and maximum receiver spacings are *20 m* and *90 m*, respectively. The corresponding optimal bandwidth for the array is *40 Hz* to *200 Hz* for P-waves and *20 Hz* to *100 Hz* for S-waves. Depending upon the array geometry and level of radial symmetry, the receiver spacing and therefore sensitivity could vary with azimuth. The array in this study is designed to be approximately radially and azimuthally symmetric, so the azimuthal sensitivity is approximately constant.

3.1.4 A note on stacking

Stacking the time-shifted waveforms within the beamforming process suppresses incoherent noise. In this study we linearly stack the data. However, one could also use nth root stacking (Rost and Thomas, 2002) or phase-weighted stacking (Schimmel and Paulssen, 1997). We find negligible differences in performance using different stacking techniques for the array setup in this study. This is likely because the array has a small (*100 m*) aperture and minimal scattering occurs within the shallow firn layer at RIS, therefore resulting in insignificant incoherent noise compared to local icequake signals, regional earthquakes and coherent ambient seismic noise sources. We would recommend reconsidering the choice of stacking method for larger aperture arrays or sites with significant near-surface heterogeneity, either of which would increase incoherent noise levels.

3.2 Network-based icequake detection and location

The array-based detection and location method presented in this study is benchmarked against a current state-of-the-art method for network-based icequake detection, QuakeMigrate (Hudson et al., 2019). This method approximates the energy from an icequake arriving at each receiver with a Gaussian onset function, which are then back-migrated through time and space to search for a coalescence of energy that corresponds to an event. If a sufficiently high coalescence of energy is found over a

https://doi.org/10.5194/egusphere-2023-657
Preprint. Discussion started: 12 April 2023

particular time window, then it triggers an event detection. Full details on this method can be found in Hudson et al. (2019). Although this method inherently provides an estimate of hypocentral location for each event, we relocate all events using the non-linear icequake location algorithm NonLinLoc (Lomax and Virieux, 2000). The QuakeMigrate method shares similarities with the beamforming method (see Section 3.1), with both seeking to identify coherent arrivals of energy within a particular frequency bandwidth. The key difference between the two is that the array-based method searches a pre-defined slowness-azimuth space, which in this case is undertaken in the fk-domain, while the network-based approach searches over a pre-defined 3D spatial grid through time.

3.3 Moment magnitude

One can use the icequake magnitude distribution to quantify the performance of the array compared to the network. We choose to use moment magnitude, M_w (Hanks and Kanamori, 1979), as it provides an absolute measure of the actual moment release of an icequake, rather than relying on an empirical relationship. Another benefit is that unlike local magnitude scales, it doesn′t exhibit a break in the scaling relationship at low magnitudes ($M_w < 3$) (Deichmann, 2017; Hudson et al., 2022). Moment magnitudes are calculated using SeisSrcMoment (Hudson, 2020) (see Hudson et al. (2022) for details on applying the method). This involves fitting a Brune model (Brune, 1970) to the frequency spectrum of the icequake.

4 Results and discussion

4.1 Icequake detection using arrays vs. networks

Detected icequake hypocentres are shown in Figure 4, with a summary of the magnitude distribution of these icequakes shown in Figure 5. The magnitude distributions for three setups are shown in Figure 5: (1) the array-based detection method applied to the array shown in Figure 1d (Figure 5b); (2) the network-based detection method applied to the same array shown in Figure 1d (green points, Figure 5a); and the network-based detection method applied to the entire network shown in Figure 1c (red points, Figure 5a). The results therefore allow for the comparison of an array deployment to a network deployment, as well as an array-based vs. network-based detection and location algorithms more generally.

The array-based detection outperforms the network-based detection method in several areas. Firstly, the array detects an order of magnitude more icequakes than the network (see Figure 5). The additional icequake detections in the array data originate both near the array and greater distances from the array/network centre than icequakes detected using the network-based approach. Icequakes continue to be detected at distances of 10 km or more, albeit with an increasing average magnitude with distance, whereas the network has a sharp detection limit at ~ 7.5 km from the network centre (see Figure 5d). Additionally, the array detects $\sim$*10,000* icequakes with magnitudes > 0, whereas the network only detects a negligible number of these larger icequakes, many of which originate far outside the spatial extent of the network (see Figure 5).

However, the network-based detection outperforms the array-based detection method in other ways. Firstly, the network-based method detects a higher proportion of the smaller icequakes, with a magnitude of completeness, $M_{c,network} = -0.81$,

https://doi.org/10.5194/egusphere-2023-657
Preprint. Discussion started: 12 April 2023

compared to $M_{c,array} = -0.49$ for the array-based method. Furthermore, it is easier to filter the network-based method for false-triggers. This is evidenced by the clustering of seismicity at sticky-spots clearly exhibited in the network-based event locations (Figure 4c) but not as clearly in the array-based data (Figure 4a).

Overall, the array-based method is more sensitive than the network-based method, detecting more icequakes across the magnitude range. This result is likely for two reasons. Firstly, the array-based method outperforms the network-based approach for phase association, with multiple P- and S- wave phase arrivals possible to associate within a given time-window. This is possible due to the accuracy of back-azimuth measurements, allowing arrivals with back-azimuths with differences $< 10^o$ to be paired, even if phase arrivals overlap. This is particularly powerful when accounting for radiation pattern effects, as shown in Figure 3. For the example in Figure 3, two events close in time originating from different back-azimuths have inverse P/S amplitude ratios, due to radiation pattern effects, yet are both detected within the same window. Theoretically, tens of events could overlap within each time window, limited only by the back-azimuth tolerance and distribution of event back-azimuths. This is in contrast to the network-based approach, where only one event association would be allowed within a given time window, so as to minimise the risk of incorrect phase associations. However, the greater number of events detected by the array-based method could also be due a lack of metrics to filter the catalogue by. Although our array-processing method provides uncertainty estimates, these have a particularly coarse temporal resolution, limiting their use for filtering the data to remove false event detections. Conversely, the network-based approach measures uncertainty with a higher resolution, allowing both temporal and spatial uncertainty filters to be used to remove false detections. However, given our strict ($< 10^o$) back-azimuth phase association criterion, we are confident that the difference between the array-based and network-based methods is not solely due to false event triggering.

4.1.1 A note on icequake magnitude distributions

Tectonic earthquake magnitudes typically follow a logarithmic scaling relationship (Gutenberg and Richter, 1936, 1944). The array-based icequake detection results shown in Figure 5b exhibit a similar relationship, with the tail-off at magnitudes below the magnitude of completeness, M_c, caused by icequake signal-to-noise (SNR) ratios falling below the noise level, leading to not all events being detected. However, the network-based icequake magnitude distributions do not exhibit a clear linear trend (see Figure 5a). This effect is not caused by S-wave anisotropy or assumptions about the source mechanism orientation, with P-wave M_w and average moment-tensor M_w distributions exhibiting similar peaks and troughs in the binned data. We instead find that these peaks and troughs in the M_w distribution are caused by spatially-distinct icequake clusters with their own narrow magnitude distributions (see Figure 5c). The limited extent of magnitude variation for each cluster is presumably governed by bed properties, whether that be the extent of slip, the rupture velocity of the ice-bed interface, or other similar effects (Gräff and Walter, 2021; Hudson et al., 2023; Zoet et al., 2012). This clustered distribution of icequakes also likely plays a role in mean M_w with distance (see Figure 5d), where the network is more sensitive to small icequakes in clusters within within the network extent. The array-based detection results do not exhibit this cluster-dominated behaviour since it can detect events at greater distances, therefore sampling a greater distribution of icequake clusters and potentially icequake sources (perhaps including crevassing as well as basal icequakes).

https://doi.org/10.5194/egusphere-2023-657
Preprint. Discussion started: 12 April 2023

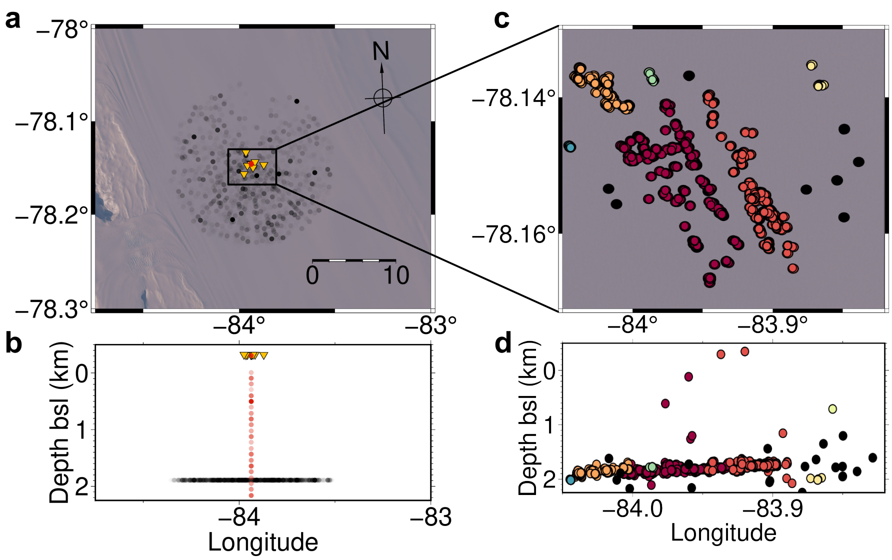

Figure 4. (a), (b) Array derived icequake catalogue hypocentres. Red points are using the full 3D array location method. Grey points are using the fixed depth method. (c), (d) Network derived icequake catalogue hypocentres, coloured by icequake cluster (see text for details).

4.2 Icequake location using arrays vs. networks

The network outperforms the array for icequake location. This is evident from the clearly discernible icequake clusters in the network-based icequake catalogue shown in Figure 4c, expected at RIS based on findings from the same area of bed when a much denser seismic network was deployed (Kufner et al., 2021). Similar observations are obtained when locating the icequakes only using the ten inner array stations with the network-based location method. Icequake clustering is indiscernible in the array-based icequake location results in Figure 4a. One reason for this is the filtering of high quality icequake phase arrivals in the network data using temporal and spatial uncertainty measurements, as described in Hudson et al. (2019). Noisy, poorly-constrained yet real icequakes are likely filtered out by definition in the network-based results whereas these noisier, low SNR icequakes may be kept in the array-based results. This could also affect the behaviour of M_w with distance (see Figure 5d).

However, there is also a more fundamental limitation in the location results of the array-based method: the presence of a near-surface, low-velocity firn layer (Smith et al., 2020; Zhou et al., 2022) that causes seismic waves to steeply dip towards the surface (see Figure 2). Glacier settings with a thinner or no firn layer would result in better constraint of event location. Uncertainty in the velocity structure of the firn layer, especially at P-wave wavelengths ($< 10\ m$) limits the measurement of takeoff angle from apparent slowness used in the array-based method′s 3D icequake location procedure. This is what causes the icequakes located using the array-based method to be miss-located directly beneath the array (red scatter points, Figure 4a,b). To mitigate this issue, we are forced to neglect firn layer effects, and project icequake epicentres onto an artificial horizontal plane at approximately the depth of the ice-bed interface using the fixed-depth location method (see Figure 2f). Obviously

https://doi.org/10.5194/egusphere-2023-657
Preprint. Discussion started: 12 April 2023

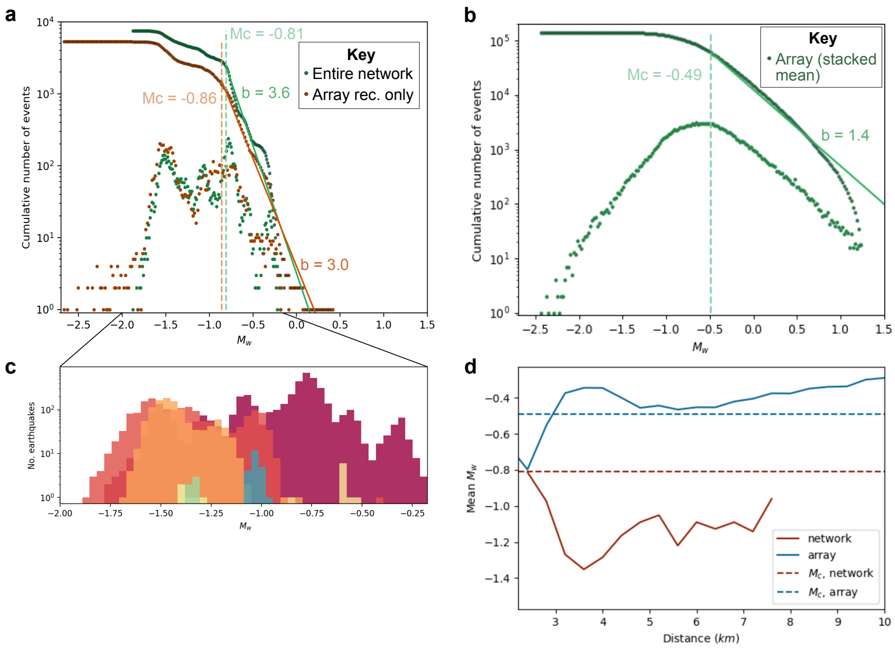

Figure 5. a. Moment magnitude distribution for entire network and array stations only, with events detected using migration-based method. b. Same as (a) but for array using array-based detection method (using the fixed-depth hypocentres, see Figure 4), and the mean of the linearly-stacked waveform data from the array. c. Plot of histogram-binned data for individual spatial icequake clusters from the entire network data from (a). Data are coloured to corresponding clusters in Figure 4c. d. Plot of mean M_w with distance from the array/network centre for the entire network data from (a) and the array data from (b). Note: magnitudes of completeness are fixed with distance in (d), and included for indicative purposes only.

this is an approximation, with both neglecting the firn layer and differences between the average ice-bed interface and the true icequake depth resulting in greater uncertainty in the icequake epicentres, likely making any icequake clusters impossible to discern. High resolution ($< 10\ m$) 3D imaging (lateral in addition to vertical) of the firn velocity structure beneath the array could allow one to apply an array transfer function to minimise these effects, although without access to such data we cannot test this hypothesis.

4.3 New insights into Rutford Ice Stream

The array deployment provides new insight into seismicity at RIS.

Previous studies of RIS suggest that bed properties vary upstream of the deployment vs. downstream (Smith, 1997; Smith and Murray, 2009). The upstream bed is thought to be comprised of unconsolidated sediment that fails aseismically, while the bed downstream can fail seismically at sticky-spots (Smith et al., 2015) (see Figure 1). Kufner et al. (2021) use a larger network of 35 receivers to find icequakes upstream of the seismic-aseismic boundary (blue points and purple line, respectively,

https://doi.org/10.5194/egusphere-2023-657
Preprint. Discussion started: 12 April 2023

Figure 6), interpreted to occur in the depressions of Mega-Scale Glacier Lineations (MSGLs) in the previously aseismic region. Array-processing enables event detection at greater hypocentral distances, allowing us to confirm the findings of Kufner et al. (2021), with seismicity extending further upstream again, likely only limited by array sensitivity and the maximum $\Delta t_{P-S,max}$ time that we impose for P-S phase association. To this end, we increase $\Delta t_{P-S,max}$ to *10 s* to search for more distal events (red points, Figure 6), although this catalogue is dominated by false triggers due to incorrect phase associations caused by significant variation in back-azimuth within such a large time-window. Figure 6b shows an example of an upstream event from the $\Delta t_{P-S,max} = 2.5s$ catalogue. The icequake has a high SNR P-wave arrival but a low SNR S-wave arrival, characteristic of a double-couple stick-slip icequake with a ray takeoff angle of $\sim 45^o$, consistent with the icequake hypocentre. This low S-wave SNR is present on all network stations, which are all a similar distance and azimuth from the icequake, is likely why the network-based method fails to detect the event. An additional interesting feature is the aseismic gap present in both the Kufner et al. (2021) icequake catalogue and more clearly in the array-processing catalogue, at azimuths of $\sim -5^oN$ to $\sim 20^oN$ (green zone, Figure 6). Observing seismicity in the previously inferred aseismic region has implications for bed complexity and icequake nucleation, potentially supporting ideas such as basal water pressures modulating bed friction and seismicity (Hudson et al., 2023; Gräff et al., 2021).

The second observation in the array results that we emphasise here are icequakes at the shear-margins of RIS. Again, these events are observed due to the greater detection distances of array-based methods (up to 20 km) compared to networks (< 10 km). Two icequakes are highlighted, one at the limit of the $\Delta t_{P-S,max} < 2.5s$ catalogue (Figure 6c) and another that occurs in the $\Delta t_{P-S,max} < 10s$ (Figure 6d) catalogue. The P and S arrivals of these icequakes are significantly different to typical basal icequakes at RIS, with the events occurring during a much higher-amplitude, "noisier" time period, with lower SNR P- and S- wave arrivals. However, the velocity amplitudes are two orders of magnitude greater. We interpret these to be icequakes be surface or basal crevasse fracture at the shear-margin, where the ice is highly damaged. The apparent "noise" in the waveforms could actually be many crevasse icequakes occurring simultaneously, combined with at least some scattering of seismic waves off existing fractures within the shear-margin. Such icequakes could provide information on shear-margin dynamics, such as how important damage to the ice fabric is for impeding or accelerating ice stream flow.

4.4 Lessons learnt and recommendations for using arrays in the cryosphere

1. *Seismic networks are more sensitive than arrays for studying smaller areas in more detail.* The network-based approach had a smaller magnitude of completeness than the array-based approach, while also providing greater spatial constraint of icequake hypocentres that allow clusters of events to be identified. For studying a particular glaciological process in as much detail/as comprehensively as possible, we recommend deploying a seismic network rather than an array. This is especially true for sites with a thick (greater than seismic wavelength) low-velocity firn-layer.

2. *Arrays can detect icequakes at greater distances than networks.* Arrays can outperform networks for detecting events, especially when P- and S-wave phase arrivals overlap in time. Theoretically, the array-processing method here can detect many events within a given time-window, compared to a single event using the network method. Furthermore, phases

https://doi.org/10.5194/egusphere-2023-657
Preprint. Discussion started: 12 April 2023

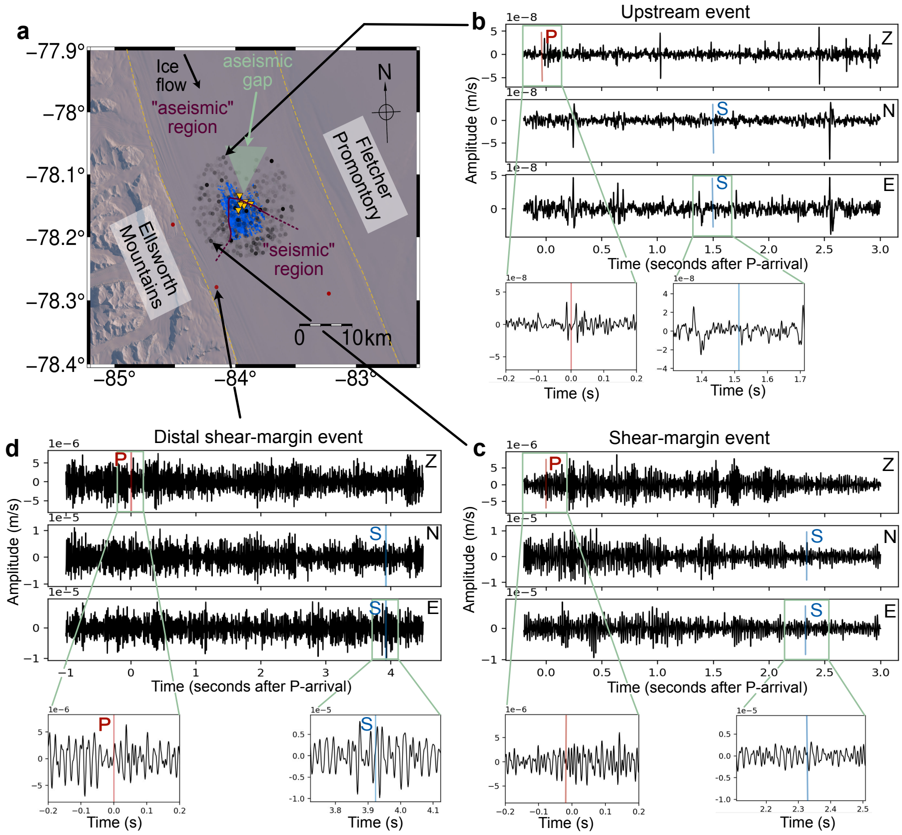

Figure 6. Examples of previously unobserved icequakes at Rutford Ice Stream. a. Map of overall seismicity detected in this study within the context of RIS more widely. Grey points are the icequake catalogue from array-processing in this study with $\Delta t_{P-S,max} = 2.5s$, red points are for an array-processing catalogue with $\Delta t_{P-S,max} = 10s$ (only events $> 0.8 P_{max}$), blue points are icequakes from Kufner et al. (2021), the yellow dashed lines indicate the shear-margins and the purple solid-dashed line indicates the boundary between the previously inferred seismic-aseismic reion (Smith, 1997; Smith and Murray, 2009). b. Example icequake located upstream, in the "aseismic" region from the $\Delta t_{P-S,max} = 2.5s$ icequake catalogue. c. Shear-margin icequake from the $\Delta t_{P-S,max} = 2.5s$ icequake catalogue. d. Distal shear-margin icequake from the $\Delta t_{P-S,max} = 10s$ icequake catalogue.

from an event that have highly differing SNRs can still be readily associated as from the same event. Together, these properties of the array-processing method enable more events to be detected from greater distances, and during noisier time periods. We therefore suggest that arrays are useful for initial scoping of a field site, before potentially deploying a more comprehensive network to study a particular process.

3. *Arrays typically require fewer instruments than a network.* The array in this study comprised of only ten receivers, whereas ideally a seismic network would comprise of tens to hundreds or more receivers. Arrays therefore provide an efficient means to investigate seismic activity, at least initially.

https://doi.org/10.5194/egusphere-2023-657
Preprint. Discussion started: 12 April 2023

4. *Array and network geometries limit detection performance in different ways.* As described above, arrays and networks have different advantages and compromises. Arrays require receiver spacings optimised to the spectral-content of the earthqaukes to be detected, which may not be known in advance. In this study that spacing is *20 m* to *90 m*. In contrast, networks generally perform best when receivers are evenly spaced, with icequake depths are not greater than the maximum receiver spacing. The optimal receiver spacing for a network to study basal icequakes at RIS ($\sim 2\ km$) is therefore much greater than the maximum optimal array receiver spacing ($\sim 100\ m$). To summarise, it is challenging to design a deployment optimised for both array and network processing.

5. *Consider networks of sub-arrays to capitalise on the advantages of both network and arrays.* If one has a sufficient number of receivers, then it may be possible to deploy sub-arrays, evenly spaced within an overall network. This could facilitate a hybrid detection approach, taking advantage of both network and array benefits.

5 Conclusions

Here, we focus on how useful array-processing is for deployments studying icequakes at glaciers, icesheets and ice shelves. The motivations for using arrays rather than networks are that the cryosphere is often challenging to access, logistically expensive to operate within and potential seismically active areas are typically highly variable temporally and spatially. Seismic arrays could facilitate smaller seismic deployments than conventional networks, while enabling event detection at greater distances. To investigate this question, the performance of an array is compared to a sparse network at RIS, Antarctica. We find that arrays can detect icequakes over a greater spatial extent than seismic networks, but provide poorer spatial constraint on seismicity within a network, where networks have the potential to elucidate glaciological processes in greater detail. We suggest a number of recommendations based on learnings from this study, especially that arrays might be particularly useful for initial scoping field deployments, or where one only has access to an insufficient number of instruments to deploy a suitable network.

Code and data availability. The beamforming method presented in this study is available as an open source python package, SeisSeeker (https://zenodo.org/badge/latestdoi/523305896). The comparison network-based method, QuakeMigrate, is also available open source (Winder et al., 2021). The seismic catalogues containing all detected events, their locations and magnitudes are available here (https://doi.org/10.5281/zenodo.7797986). Continuous seismic data for the entire experiment period will be uploaded to IRIS (NETWORK CODE and DOI tbc) upon publication.

Author contributions. AB and SK designed the experiment. TH developed the method, performed the analysis and prepared the original draft. AB and AS acquired the funding. All authors contributed to the review and editing of the manuscript.

https://doi.org/10.5194/egusphere-2023-657
Preprint. Discussion started: 12 April 2023

Competing interests. The authors have no competing interests.

Acknowledgements. We thank C. Thomas for her advice on designing the array geometry. We thank the authors of Bowden et al. (2021) for sharing python notebooks that inspired the underlying beamforming algorithm used in this work. We highly recommend that those interested in the method also read this work and associated python notebooks. We thank the UKRI NERC British Antarctic Survey for providing logistical support for the project, which was funded by the BEAMISH project (grants: NE/G014159/1, NE/G013187/1). The instruments used for this experiment are from the UK Geophysical Equipment Facility (GEF loan number 1111). T. Hudson was funded by The Leverhulme Trust via a Leverhulme Early Career Fellowship (ECF-2022-499).

https://doi.org/10.5194/egusphere-2023-657
Preprint. Discussion started: 12 April 2023

References

Aster, R. C. and Winberry, J. P.: Glacial seismology, Reports on Progress in Physics, 80, https://doi.org/10.1088/1361-6633/aa8473, 2017.

Bowden, D. C., Sager, K., Fichtner, A., and Chmiel, M.: Connecting beamforming and kernel-based noise source inversion, Geophysical Journal International, 224, 1607–1620, https://doi.org/10.1093/gji/ggaa539, 2021.

Bowers, D. and Selby, N. D.: Forensic seismology and the comprehensive nuclear-test-ban treaty, Annual Review of Earth and Planetary Sciences, 37, 209–236, https://doi.org/10.1146/annurev.earth.36.031207.124143, 2009.

Brune, J. N.: Tectonic Stress and the Spectra of Seismic Shear Waves from Earthquakes, Journal of Geophysical Research, 75, 4997–5009, 1970.

Cooley, J., Winberry, P., Koutnik, M., and Conway, H.: Tidal and spatial variability of flow speed and seismicity near the grounding zone of Beardmore Glacier, Antarctica, Annals of Glaciology, 60, 37–44, https://doi.org/10.1017/aog.2019.14, 2019.

Deichmann, N.: Theoretical basis for the observed break in ML/MW scaling between small and large earthquakes, Bulletin of the Seismological Society of America, 107, 505–520, https://doi.org/10.1785/0120160318, 2017.

Ekström, G.: Global detection and location of seismic sources by using surface waves, Bulletin of the Seismological Society of America, 96, 1201–1212, https://doi.org/10.1785/0120050175, 2006.

Ekström, G., Nettles, M., and Abers, G. A.: Glacial Earthquakes, Science, 302, 622–624, https://doi.org/10.1126/science.1088057, 2003.

Fretwell, P., Pritchard, H. D., Vaughan, D. G., Bamber, J. L., Barrand, N. E., Bell, R., Bianchi, C., Bingham, R. G., Blankenship, D. D., Casassa, G., Catania, G., Callens, D., Conway, H., Cook, A. J., Corr, H. F., Damaske, D., Damm, V., Ferraccioli, F., Forsberg, R., Fujita, S., Gim, Y., Gogineni, P., Griggs, J. A., Hindmarsh, R. C., Holmlund, P., Holt, J. W., Jacobel, R. W., Jenkins, A., Jokat, W., Jordan, T., King, E. C., Kohler, J., Krabill, W., Riger-Kusk, M., Langley, K. A., Leitchenkov, G., Leuschen, C., Luyendyk, B. P., Matsuoka, K., Mouginot, J., Nitsche, F. O., Nogi, Y., Nost, O. A., Popov, S. V., Rignot, E., Rippin, D. M., Rivera, A., Roberts, J., Ross, N., Siegert, M. J., Smith, A. M., Steinhage, D., Studinger, M., Sun, B., Tinto, B. K., Welch, B. C., Wilson, D., Young, D. A., Xiangbin, C., and Zirizzotti, A.: Bedmap2: Improved ice bed, surface and thickness datasets for Antarctica, Cryosphere, 7, 375–393, https://doi.org/10.5194/tc-7-375-2013, 2013.

Gräff, D. and Walter, F.: Changing friction at the base of an Alpine glacier, Scientific Reports, 11, 1–10, https://doi.org/10.1038/s41598-021-90176-9, 2021.

Gräff, D., Köpfli, M., Lipovsky, B. P., Selvadurai, P. A., Farinotti, D., and Walter, F.: Fine Structure of Microseismic Glacial Stick-Slip, Geophysical Research Letters, 48, https://doi.org/10.1029/2021GL096043, 2021.

Gutenberg, B. and Richter, C. F.: Magnitude and energy of earthquakes, Science, 83, 183–185, 1936.

Gutenberg, B. and Richter, C. F.: Frequency of earthquakes in California, Bulletin of the Seismological society of America, 34, 185–188, https://doi.org/10.1038/156371a0, 1944.

Hanks, T. C. and Kanamori, H.: A moment magnitude scale, Journal of Geophysical Research, 84, 2348, https://doi.org/10.1029/JB084iB05p02348, 1979.

Hudson, T.: TomSHudson/SeisSrcMoment: First formal release (Version 1.0.0), Zenodo, https://doi.org/http://doi.org/10.5281/zenodo.4010325, 2020.

Hudson, T., Kufner, S., Brisbourne, A., Kendall, J., Smith, A., Arthern, R., and Alley, R.: Friction and slip measured at the bed of an Antarctic ice stream, Nature Geoscience, https://doi.org/10.21203/rs.3.rs-1214097/v1, 2023.

Hudson, T. S., Smith, J., Brisbourne, A. M., and White, R. S.: Automated detection of basal icequakes and discrimination from surface crevassing, Annals of Glaciology, 60, 167–181, https://doi.org/10.1017/aog.2019.18, 2019.

https://doi.org/10.5194/egusphere-2023-657
Preprint. Discussion started: 12 April 2023

Hudson, T. S., Brisbourne, A. M., Walter, F., Gräff, D., White, R. S., and Smith, A. M.: Icequake Source Mechanisms for Studying Glacial Sliding, Journal of Geophysical Research: Earth Surface, 125, https://doi.org/10.1029/2020JF005627, 2020.

Hudson, T. S., Baird, A. F., Kendall, J. M., Kufner, S. K., Brisbourne, A. M., Smith, A. M., Butcher, A., Chalari, A., and Clarke, A.: Distributed Acoustic Sensing (DAS) for Natural Microseismicity Studies: A Case Study From Antarctica, Journal of Geophysical Research: Solid Earth, 126, 1–19, https://doi.org/10.1029/2020jb021493, 2021.

Hudson, T. S., Kendall, J.-M., Pritchard, M. E., Blundy, J. D., and Gottsmann, J. H.: From slab to surface: Earthquake evidence for fluid migration at Uturuncu volcano, Bolivia, Earth and Planetary Science Letters, 577, 117 268, https://doi.org/10.1016/j.epsl.2021.117268, 2022.

Jerkins, A. E., Köhler, A., and Oye, V.: On the potential of offshore sensors and array processing for improving seismic event detection and locations in the North Sea, Geophysical Journal International, 233, 1191–1212, https://doi.org/10.1093/gji/ggac513, 2023.

Klaasen, S., Paitz, P., Lindner, N., Dettmer, J., and Fichtner, A.: Distributed Acoustic Sensing in Volcano-Glacial Environments—Mount Meager, British Columbia, Journal of Geophysical Research: Solid Earth, 126, 1–17, https://doi.org/10.1029/2021JB022358, 2021.

Köpfli, M., Gräff, D., Lipovsky, B. P., Selvadurai, P. A., Farinotti, D., and Walter, F.: Hydraulic Conditions for Stick-Slip Tremor Beneath an Alpine Glacier, Geophysical Research Letters, 49, 1–11, https://doi.org/10.1029/2022gl100286, 2022.

Kufner, S., Brisbourne, A. M., Smith, A. M., Hudson, T. S., Murray, T., Schlegel, R., Kendall, J. M., Anandakrishnan, S., and Lee, I.: Not all Icequakes are Created Equal: Basal Icequakes Suggest Diverse Bed Deformation Mechanisms at Rutford Ice Stream, West Antarctica, Journal of Geophysical Research: Earth Surface, 126, https://doi.org/10.1029/2020JF006001, 2021.

Lindner, F., Walter, F., Laske, G., and Gimbert, F.: Glaciohydraulic seismic tremors on an Alpine glacier, Cryosphere, 14, 287–308, https://doi.org/10.5194/tc-14-287-2020, 2020.

Lipovsky, B. P., Meyer, C. R., Zoet, L. K., McCarthy, C., Hansen, D. D., Rempel, A. W., and Gimbert, F.: Glacier sliding, seismicity and sediment entrainment, Annals of Glaciology, 60, 182–192, https://doi.org/10.1017/aog.2019.24, 2019.

Löer, K., Riahi, N., and Saenger, E. H.: Three-component ambient noise beamforming in the Parkfield area, Geophysical Journal International, 213, 1478–1491, https://doi.org/10.1093/GJI/GGY058, 2018.

Lomax, A. and Virieux, J.: Probabilistic earthquake location in 3D and layered models, Advances in Seismic Event Location, Volume 18 of the series Modern Approaches in Geophysics, pp. 101–134, 2000.

McBrearty, I. W., Zoet, L. K., and Anandakrishnan, S.: Basal seismicity of the Northeast Greenland Ice Stream, Journal of Glaciology, pp. 1–17, https://doi.org/10.1017/jog.2020.17, 2020.

Näsholm, S. P., Iranpour, K., Wuestefeld, A., Dando, B. D., Baird, A. F., and Oye, V.: Array Signal Processing on Distributed Acoustic Sensing Data: Directivity Effects in Slowness Space, Journal of Geophysical Research: Solid Earth, 127, 1–24, https://doi.org/10.1029/2021JB023587, 2022.

Podolskiy, E. A. and Walter, F.: Cryoseismology, Reviews of Geophysics, 54, 1–51, https://doi.org/10.1002/2016RG000526, 2016.

Pratt, M. J., Winberry, J. P., Wiens, D. A., Anandakrishnan, S., and Alley, R. B.: Seismic and geodetic evidence for grounding-line control of Whillans Ice Stream stick-slip events, Journal of Geophysical Research: Earth Surface, 119, 333–348, https://doi.org/10.1002/2013JF002842, 2014.

Roeoesli, C., Helmstetter, A., Walter, F., and Kissling, E.: Meltwater influences on deep stick-slip icequakes near the base of the Greenland Ice Sheet, Journal of Geophysical Research: Earth Surface, 121, 223–240, https://doi.org/10.1002/2015JF003601, 2016.

Rost, S. and Thomas, C.: Array seismology: Methods and applications, Reviews of Geophysics, 40, 2–1–2–27, https://doi.org/10.1029/2000RG000100, 2002.

Schimmel, M. and Paulssen, H.: Noise reduction and detection of weak, coherent signals through phase-weighted stacks, Geophysical Journal International, 130, 497–505, https://doi.org/10.1111/j.1365-246X.1997.tb05664.x, 1997.

Smith, A. M.: Basal conditions on Rufford Ice Stream, West Antarctica, from seismic observations, Journal of Geophysical Research, 102, 543–552, 1997.

Smith, A. M.: Microearthquakes and subglacial conditions, Geophysical Research Letters, 33, 1–5, https://doi.org/10.1029/2006GL028207, 2006.

Smith, A. M. and Murray, T.: Bedform topography and basal conditions beneath a fast-flowing West Antarctic ice stream, Quaternary Science Reviews, 28, 584–596, https://doi.org/10.1016/j.quascirev.2008.05.010, 2009.

Smith, A. M., Anker, P. G., Nicholls, K. W., Makinson, K., Murray, T., Rios-Costas, S., Brisbourne, A. M., Hodgson, D. A., Schlegel, R., and Anandakrishnan, S.: Ice stream subglacial access for ice-sheet history and fast ice flow: The BEAMISH Project on Rutford Ice Stream, West Antarctica and initial results on basal conditions, Annals of Glaciology, https://doi.org/10.1017/aog.2020.82, 2020.

Smith, E., Smith, A., White, R., Brisbourne, A., and Pritchard, H.: Mapping the ice-bed interface characteristics of Rutford Ice Stream, West Antarctica, using microseismicity, Journal of Geophysical Research: Earth Surface, 120, 1881–1894, https://doi.org/10.1002/2015JF003587, 2015.

Tsai, V. C. and Ekström, G.: Analysis of glacial earthquakes, Journal of Geophysical Research, 112, F03S22, https://doi.org/10.1029/2006JF000596, 2007.

Umlauft, J., Lindner, F., Roux, P., Mikesell, T. D., Haney, M. M., Korn, M., and Walter, F. T.: Stick-Slip Tremor Beneath an Alpine Glacier, Geophysical Research Letters, 48, 1–10, https://doi.org/10.1029/2020GL090528, 2021.

Van Den Ende, M. P. and Ampuero, J. P.: Evaluating seismic beamforming capabilities of distributed acoustic sensing arrays, Solid Earth, 12, 915–934, https://doi.org/10.5194/se-12-915-2021, 2021.

Wang, W. and Vidale, J. E.: An initial map of fine-scale heterogeneity in the Earth's inner core, Nature Geoscience, 15, 240–244, https://doi.org/10.1038/s41561-022-00903-8, 2022.

Winder, T., Bacon, C., Smith, J. D., Hudson, T. S., Drew, J., and White, R. S.: QuakeMigrate v1.0.0, Zenodo, https://doi.org/10.5281/zenodo.4442749, 2021.

Wolf, J., Frost, D. A., Long, M. D., Garnero, E., Aderoju, A. O., Creasy, N., and Bozdağ, E.: Observations of Mantle Seismic Anisotropy Using Array Techniques: Shear-Wave Splitting of Beamformed SmKS Phases, Journal of Geophysical Research: Solid Earth, 128, https://doi.org/10.1029/2022JB025556, 2023.

Zhou, W., Butcher, A., Brisbourne, A. M., Kufner, S. K., Kendall, J. M., and Stork, A. L.: Seismic Noise Interferometry and Distributed Acoustic Sensing (DAS): Inverting for the Firn Layer S-Velocity Structure on Rutford Ice Stream, Antarctica, Journal of Geophysical Research: Earth Surface, 127, 1–17, https://doi.org/10.1029/2022JF006917, 2022.

Zoet, L. K., Anandakrishnan, S., Alley, R. B., Nyblade, A. A., and Wiens, D. A.: Motion of an Antarctic glacier by repeated tidally modulated earthquakes, Nature Geoscience, 5, 623–626, https://doi.org/10.1038/ngeo1555, 2012.

Zoet, L. K., Carpenter, B., Scuderi, M., Alley, R. B., Anandakrishnan, S., Marone, C., and Jackson, M.: The effects of entrained debris on the basal sliding stability of a glacier, Journal of Geophysical Research: Earth Surface, 118, 656–666, https://doi.org/10.1002/jgrf.20052, 2013.